ARTICLES

Trajectory Study of Supercollision Relaxation in Highly Vibrationally Excited Pyrazine and CO_2

Ziman Li, Rebecca Sansom, Sara Bonella, David F. Coker, and Amy S. Mullin*

Department of Chemistry, Boston University, Boston, Massachusetts 02215

Received: May 13, 2005; In Final Form: June 27, 2005

Classical trajectory calculations were performed to simulate state-resolved energy transfer experiments of highly vibrationally excited pyrazine (E_{vib} = 37 900 cm^{-1}) and CO_2, which were conducted using a high-resolution transient infrared absorption spectrometer. The goal here is to use classical trajectories to simulate the supercollision energy transfer pathway wherein large amounts of energy are transferred in single collisions in order to compare with experimental results. In the trajectory calculations, Newton's laws of motion are used for the molecular motion, isolated molecules are treated as collections of harmonic oscillators, and intermolecular potentials are formed by pairwise Lennard-Jones potentials. The calculations qualitatively reproduce the observed energy partitioning in the scattered CO_2 molecules and show that the relative partitioning between bath rotation and translation is dependent on the moment of inertia of the bath molecule. The simulations show that the low-frequency modes of the vibrationally excited pyrazine contribute most to the strong collisions. The majority of collisions lead to small ΔE values and primarily involve single encounters between the energy donor and acceptor. The large ΔE exchanges result from both single impulsive encounters and chattering collisions that involve multiple encounters.

I. Introduction

Highly vibrationally excited molecules are important in many nonequilibrium processes such as combustion and atmospheric photochemistry. The collisional relaxation of such species is fundamental as a competing pathway to unimolecular decomposition and isomerization reactions. A number of experimental studies[1−7] have been performed on the relaxation of highly vibrationally excited aromatic molecules with $E_{vib} \sim$ 20000−40000 cm^{-1}, but none have been able to provide a detailed measure of the relaxation process through the eyes of the hot molecule. This is because the vibrational state densities at these energies are far too large to allow access to state-resolved information. Pyrazine with E_{vib} = 37 900 cm^{-1}, for example, has a state density of $\rho \sim 10^{12}$ vibrational states per cm^{-1}, precluding the effective use of traditional spectroscopies. Over the past decade, experiments done in the Flynn labs[8−13] and in our labs[14−20] have used high-resolution transient IR absorption probing to measure the state-resolved energy gain in small bath molecules that quench highly vibrationally excited aromatic molecules. These studies have revealed a great deal of information about the mechanisms through which high-energy molecules relax, but they still leave a number of unanswered questions about how the highly excited donor molecules behave during the energy transfer process. In the work presented here, we use classical trajectory methods to complement our state-resolved experimental studies[14,16] in order to better understand the relaxation process from the hot molecules' perspective.

Many trajectory simulation studies of collisional energy transfer[3,21−36] have focused on excited polyatomic molecules with inert atomic gases. Recent trajectory investigations[24,37−43] have studied collisional energy transfer between highly excited polyatomic donor molecules and polyatomic bath molecules, including a number of studies that focused on the collisional relaxation of vibrationally excited pyrazine. Chapman et al.[41,42] investigated the collisional energy transfer between highly excited pyrazine (E_{vib} = 40 332 cm^{-1}) molecules and CO bath molecules. Their calculation results showed qualitative agreement with the diode laser experiments of Flynn and co-workers[44] and indicated that energy-transfer properties depend on the initial rotational state of the CO. Luther et al.[38,39] conducted trajectory calculations for the collisional quenching of hot pyrazine with various polyatomic colliders and investigated the temperature dependence of collisional energy transfer. Luther's studies highlight the importance of pyrazine rotational energy gain as part of the supercollision relaxation process. Barker and co-workers[43] investigated vibrational relaxation in collisions between pyrazine and argon and found that only a small fraction of the available vibrational energy is transferred to recoil energy, which was in good agreement with their experimental data.[45]

One focus of our trajectory calculations is to investigate the effect of the donor molecule's vibrational structure on the partitioning of rotational and translational energy gain that has been observed in pyrazine/CO_2 supercollisions. There has been some debate in the literature about the source of supercollisions energy transfer involving atomic collision partners. When studying collisions of hot azulene ($C_{10}H_8$) with xenon atoms,

* To whom correspondence should be addressed. E-mail: mullin@umd.edu. Current address: Department of Chemistry and Biochemistry, University of Maryland, College Park, Maryland 20742.

10.1021/jp0525336 CCC: $30.25
Published on Web 08/05/2005

Gilbert and co-workers postulated that the C−H stretches were the most important for energy transfer.[21] Later, when studying benzene and helium collisions, they proposed that low-frequency modes, specifically out-of-plane motions, were responsible for enhanced energy-transfer efficiency.[23] Luther and co-workers concluded that low-frequency modes were responsible for the increased energy-transfer efficiency of hexafluorobenzene relative to benzene in collisions with noble gases.[24] In trajectory studies of collisional relaxation of highly excited benzene (E_{vib} = 40 700 cm^{-1}) with cold argon and cold benzene, Bernshtein and Oref[37] found out that the gateway modes, through which energy is transferred from the excited molecules, are the low-frequency out-of-plane vibrations for both collision systems. To investigate the modes involved in pyrazine/CO_2 supercollision energy transfer, we have prepared four different sets of pyrazine molecules with different vibrational characteristics and performed classical trajectory calculations to study collisions with CO_2, specifically those that involved large changes in energy.

Another goal of these trajectory calculations is to study the effects of the mass and moment of inertia of the bath molecule on supercollisions. Barker and Miller[4] studied the collisional deactivation of vibrationally excited pyrazine by 19 collider gases using time-resolved IR fluorescence and found that overall collisional energy transfer from hot pyrazine generally increases as a function of collider mass. Zalesskaya et al.[46] used time-resolved delayed fluorescence to study how the mass of bath species affects collisional energy transfer from vibrationally excited polyatomic molecules (acetophenone, benzophenone, and anthraquinone) to a number of bath gases (Ar, C_2H_4, SF_6, CCl_4, and C_5H_{12}). Their results indicated that for $V \rightarrow V$ energy transfer, rates, and efficiencies increase as the complexity of the structure of the bath gas increases. For collisions involving $V \rightarrow T$ energy transfer, they found that energy-transfer efficiencies decrease upon increasing the mass of the bath species. Zalesskaya and co-workers explained these observations using Landau−Teller theory, in which the energy-transfer probability decreases with increasing the reduced mass of collision partners as $\mu^{-1/2}$. Schatz and co-workers[29] performed classical trajectory studies on collisional relaxation of highly excited CS_2 in collisions with helium and xenon and also found that the mass difference of the bath species plays an important role. The light helium collider participates in impulsive collisions, while the heavy xenon collider participates in "slow" collisions in which the two colliders interact strongly for several vibrational periods. As a result, they report that helium is a more efficient quencher than xenon. Lim[34,35] also studied mass effects in collisional energy transfer from hot toluene (E_{vib} = 41 000, 30 000, and 15 000 cm^{-1}) to helium and argon using quasi-classical trajectory simulations. He found that the amount of energy lost from hot toluene per collision was independent of the mass of the collision partner. However, rotational energy gain in toluene could be induced by increasing the mass of the atomic collision partner.

In this paper, classical trajectory calculations have been carried out to simulate the supercollision energy transfer pathway that has been observed in state-resolved energy-transfer experiments of highly vibrationally excited pyrazine (E_{vib} = 37 900 cm^{-1}) and CO_2.[14,16] The goal here is to use classical trajectories to simulate the partitioning of rotational and translational energy gain in CO_2 that results from supercollisions with vibrationally hot pyrazine. In the calculations presented here, Newton's laws of motion are used for the molecular motion, isolated molecules are treated as collections of harmonic oscillators, and intermolecular potentials are formed by pairwise Lennard-Jones potentials. The simulations investigate which modes of the vibrationally excited pyrazine contribute most to the supercollisions and how the mass and moment of inertia of the bath molecule influence supercollision energy transfer. Finally, the rotational and translational energy distributions of the trajectory data are analyzed and compared to experimental results.

II. Computational Method

Classical trajectory calculations were performed using the commercially available program VENUS96[47] to simulate collisional energy transfer from vibrationally excited pyrazine (E_{vib} = 37 900 cm^{-1}) to CO_2. The intramolecular potential for each molecule was formed by a collection of harmonic terms that describe stretches, bends, wags, and torsions, given as

$$V_{total} = \sum V_{stretch} + \sum V_{bend} + \sum V_{wag} + \sum V_{torsion} \quad (1)$$

The various vibrational potentials are represented by the equations

$$V_{stretch} = \frac{1}{2} f_r (r - r_0)^2 \quad (2)$$

$$V_{bend} = \frac{1}{2} f_\theta (\theta - \theta_0)^2$$

$$V_{wag} = \frac{1}{2} f_\alpha (\alpha - \pi)^2$$

$$V_{torsion} = V_0 \sin^2 \tau$$

where r is the bond length, θ is the bend angle, α is the wag angle, and τ is the torsional angle. The constants r_0 and θ_0 are the equilibrium bond lengths and angles, respectively. The constants f_r, f_θ, and f_α are the harmonic force constants for the vibrations. We used the parameters determined by Grigoleit[48] for the intramolecular potentials of pyrazine and CO_2. These parameters were selected to give the vibrational frequencies closest to the experimentally determined values and are listed in Supporting Information Appendices A and B. In Appendix A, parameters from Chapman[41] are also listed for comparison. The parameters used here are close to those used by Chapman and co-workers, with the exception of the bending mode force constants which are approximately twice as large as those used by Chapman. The vibrational frequencies calculated by the program are reported in Table 1 and Table 2 along with the experimental values[49,50] and mode assignments.

The intermolecular potential in our calculations was formed by a sum of simple pair Lennard-Jones potentials

$$V_{A\ldots B} = 4\epsilon_{A\ldots B}\left[\left(\frac{\sigma_{A\ldots B}}{r}\right)^{12} - \left(\frac{\sigma_{A\ldots B}}{r}\right)^{6}\right] \quad (3)$$

There are 30 pairs in the pyrazine/CO_2 collision system. The Lennard-Jones well depth ϵ and Lennard-Jones diameter σ parameters were taken from Grigoleit[48] and are listed in Supporting Information Appendix C.

Charge effects can be included in various ways. Grigolet[48] used eq 4 to describe interactions arising from partial charges in the neutral collision partners. However, tests indicate that

$$V_{A\ldots B} = 4\epsilon_{A\ldots B}\left[\left(\frac{\sigma_{A\ldots B}}{r}\right)^{12} - \left(\frac{\sigma_{A\ldots B}}{r}\right)^{6}\right] - \frac{q^2\alpha}{8\pi\epsilon_0 r^4} \quad (4)$$

the partial charge interaction terms do not significantly affect the intermolecular potential of pyrazine and collision partners. Qualitative agreement between experiment and theory is main-

TABLE 1: Normal Mode Frequencies of Pyrazine

symmetry	vibration	type	frequency, cm^{-1} [a]	frequency, cm^{-1} [b]
A_u	7	oop ring deformation[c]	370	350
B_{3u}	24	oop skeletal bend	438	418
A_g	5	ring deformation	635	602
B_{3g}	22	skeletal deformation	658	704
B_{2g}	14	oop skeletal bend	665	756
B_{3u}	23	oop C−H bend	842	785
B_{1g}	8	oop C−H bend	871	927
A_u	6	oop C−H bend	905	960
B_{2g}	13	oop C−H bend	984	983
A_g	4	ring breathing	1052	1016
B_{1u}	12	ring deformation	1059	1018
B_{2u}	18	C−H bend	1069	1063
B_{1u}	11	C−H bend	1099	1130
B_{2u}	17	ring deformation	1128	1149
A_g	3	C−H bend	1247	1233
B_{3g}	21	C−H bend	1293	1346
B_{2u}	16	C−C stretch	1518	1411
B_{1u}	10	C−C stretch	1612	1483
B_{3g}	20	C−C stretch	1699	1525
A_g	2	C−C stretch	1746	1580
B_{1u}	9	C−H stretch	3056	3012
B_{3g}	19	C−H stretch	3058	3040
A_g	1	C−H stretch	3060	3055
B_{2u}	15	C−H stretch	3061	3069

[a] Normal-mode frequencies of pyrazine from our normal-modes analysis calculation. [b] Normal-mode frequencies of pyrazine from IR experiments ref 49. [c] oop denotes out-of-plane.

TABLE 2: Vibrational Frequencies of CO_2

assignment	computational, cm^{-1} [a]	experimental, cm^{-1} [b]
OCO bend	674	667
C−O stretch	1261	1388
C−O stretch	2415	2349

[a] Vibrational frequencies of CO_2 from our normal-modes analysis calculation. [b] Vibrational frequencies of CO_2 from ref 50.

tained by employing the simple Lennard-Jones 6-12 potentials used here.

The trajectory calculations were carried out using initial conditions similar to those used in the corresponding experiments in our labs.[14] The pyrazine and CO_2 molecules were prepared with thermal distributions of translation and rotation corresponding to a temperature of 300 K. The initial conditions were sampled from a probability distribution that assumes a symmetric top geometry for pyrazine and a linear geometry for CO_2. Since this is a classical trajectory calculation, there is no actual quantization of vibrational energy. However, to be more realistic, normal mode coordinates and momenta are sampled to give vibrational energies corresponding to actual vibrational states. Once the trajectory has begun, the vibration is classical and the molecule can gain or lose any amount of available energy.

Four different initial conditions for the excited pyrazine molecules were used in order to explore different scenarios for deposing the 266 nm excitation energy into the vibrational modes of pyrazine. The first is referred to as randomized microcanonical. In this preparation, the pyrazine molecule is treated as thermal in rotation and translation, but the vibrational energy is fixed at the value of 37 900 cm^{-1}. This energy corresponds to the energy of a pyrazine molecule after it absorbs a 266 nm photon at 300 K. The energy E_i in each vibrational mode i is determined statistically using the following expression

$$E_i = [E_V^0 - \sum_j^{i-1} E_j][1 - R_i^{1/(n-1)}] \qquad (5)$$

The sampling begins at $i = 1$. E_V^0 is the total energy, R is a random number, and n is the number of classical harmonic oscillators. When the amplitude of each vibrational mode has been determined, the program compares the actual energy to the intended energy (37 900 cm^{-1}) and if the difference is less than 0.1%, then the configuration is accepted.

The other three preparations are referred to as localized low frequency, localized middle frequency, and localized high frequency. In each case, the initial vibrational energy in pyrazine was selected randomly using eq 5 and a subset of pyrazine's normal-mode frequencies. We use the example of the localized low frequency to illustrate how these initial configurations were determined. In the case of localized low-frequency molecules, only those vibrational modes with frequencies of less than 665 cm^{-1} contained vibrational energy from the "optical" excitation. The Beyer−Swinehart algorithm[51,52] was used to determine the energy in each of the low-frequency modes when the molecule has 37 900 cm^{-1} of vibrational energy. To do this, it assumes that the pyrazine has only five modes, those with frequencies of 370, 438, 635, 658, and 665 cm^{-1}. The energies calculated for the selected modes were converted into "quantum" numbers (since this is a classical calculation, quantum states do not really exist; quantum numbers simply represent certain amounts of energy) and used with eq 5 to specify initial conditions for the trajectory calculation. The calculation treats pyrazine as a full set of harmonic oscillators but populates only the selected modes with the energies determined from the algorithm. The mid-frequency preparation used only four modes of pyrazine with frequencies of 1518, 1612, 1699, and 1746 cm^{-1}. These frequencies represent the C−C and C−N stretches. The high-frequency preparation used only the 3056, 3058, 3060, and 3061 cm^{-1} modes of pyrazine, which are the C−H stretches.

The initial coordinates for the molecules were sampled from a uniform distribution of orientations. The impact parameter was sampled from a uniform field distribution, with the maximum impact parameter $b_{max} = 8$ Å. This value of b_{max} was chosen in the following way. The CO_2 rotational energy gain that resulted from collisions with hot pyrazine was determined from a set of 10 000 trajectory calculations with b values ranging from 0 to 8 Å. In a second set of 12 000 trajectory calculations, the CO_2 rotational energy gain distribution was determined with b values between 0 and 8.6 Å and yielded results within 0.3% of results from the first set. The centers of mass of pyrazine and CO_2 were initially separated by a distance of 8 Å, and the trajectories were propagated until they reached a distance of 10 Å following the point of closest approach. The trajectories were propagated using molecular dynamics techniques. An integration time step of 0.01 fs was used to ensure conservation of energy.

Besides the trajectory study of the pyrazine/CO_2 system, we also ran simulations for the pyrazine/"linear H_2O" collision system. The goal here is to study how the mass and mass distribution of the bath molecule affect collisional energy transfer. CO_2 has the mass distribution of heavy−heavy−heavy, and linearized H_2O is a light−heavy−light molecule. To gain insight into the strong collisions of light−heavy−light molecules, we gave water's mass to CO_2 and kept all other properties (intermolecular and intramolecular potentials, bond lengths and angles, etc.) the same as CO_2. This formed the basis of collisions between hot pyrazine and "linear H_2O". Similar calculations for collisions of pyrazine with "linear HOO" were also performed.

III. Results and Discussion

1. Characteristics of Energy Gain in CO_2. Classical trajectory calculations were performed to simulate collisional energy transfer from highly excited pyrazine molecules (E_{vib} = 37 900 cm^{-1}) to CO_2. Approximately 10 000 trajectory calculations were performed for each study, and the results are presented here. Unless otherwise specified, the hot pyrazine was prepared using a randomized microcanonical energy distribution. Parts a and b of Figure 1 show, respectively, the changes in pyrazine vibrational energy ΔE_{vib} and the CO_2 rotational energy ΔE_{rot} as a function of impact parameter *b*. Each data point corresponds to the outcome of one trajectory calculation. It can be seen that most collisions with impact parameters between $b = 0$ and $b = 8$ Å lead to small values of $|\Delta E_{vib}|$ and ΔE_{rot}. In some cases, however, there are large amounts of exchanged energy. For the purposes of this discussion, we define a supercollision as a collision with $|\Delta E_{vib}| = 3000$ cm^{-1}. Supercollisions are seen that result in pyrazine energy losses as large as $\Delta E_{vib} = -6000$ cm^{-1} and CO_2 rotational energy gain as large as $\Delta E_{rot} = 3000$ cm^{-1}. The likelihood of large ΔE collisions generally decreases with increasing impact parameter, which is consistent with an impulsive mechanism for energy transfer and is supported by experimental results.[9,14,16] In some cases, supercollision energy transfer is observed for impact parameters that are larger than the Lennard-Jones collision radius for pyrazine and CO_2 of 3.4 Å ($\sigma_{pyrazine} = 4.5$ Å and $\sigma_{CO2} = 2.3$ Å).[48] This observation could result from intermolecular attraction, elongated bond lengths in pyrazine due to large amounts of vibrational energy, or a combination of both factors. This finding is consistent with earlier computational studies by Gilbert and Oref[22] who found that some supercollisions involved high-impact parameter collisions wherein the bath gas interacts sequentially with atoms on the periphery of the hot molecule.

It is interesting to explore whether particular collision geometries preferentially lead to supercollisions. For atomic collision partners, the impact parameter provides a good description of the collision geometry, but the situation is more complicated for polyatomic collision partners where shape and relative orientation result in a broad range of possible interaction geometries. To guide the interpretation of the simulations for the pyrazine and CO_2 supercollision, we first consider the distribution of impact parameters as a function of energy loss ΔE_{vib} from hot pyrazine. The changes in pyrazine vibrational energy ΔE_{vib} from Figure 1a were binned to yield effective impact parameter values as a function of ΔE_{vib}. The results are plotted in Figure 2. Energy increments are 200 cm^{-1} for data with low vibrational energy loss, and the last data point corresponds to supercollisions with $|\Delta E_{vib}| > 3000$ cm^{-1}. The effective impact parameters are close to 4 Å for most energy-transfer events, and the smallest energy-transfer events result from glancing collisions with an effective impact parameter near 6 Å. Statistical analysis on the relative orientation of the collision partners has not yet been done but should provide insight into the configurations that are the most important for supercollision relaxation.

Figure 3 shows a scatter plot of the final relative translational energy and the final CO_2 rotational energy for ~10 000 trajectories. Each data point represents the outcome of one trajectory calculation. Most trajectories result in energy transfer from pyrazine vibration into CO_2 rotation and translation with E_{rot} = 1000 cm^{-1} and a relative translational energy $E_{rel} \leq 1500$ cm^{-1}. Only a small fraction of trajectories have final relative translational energy greater than 1500 cm^{-1} and CO_2 rotational energies greater than 1000 cm^{-1}. It is useful for comparison purposes to bin the rotational energy data to better illustrate the correlation

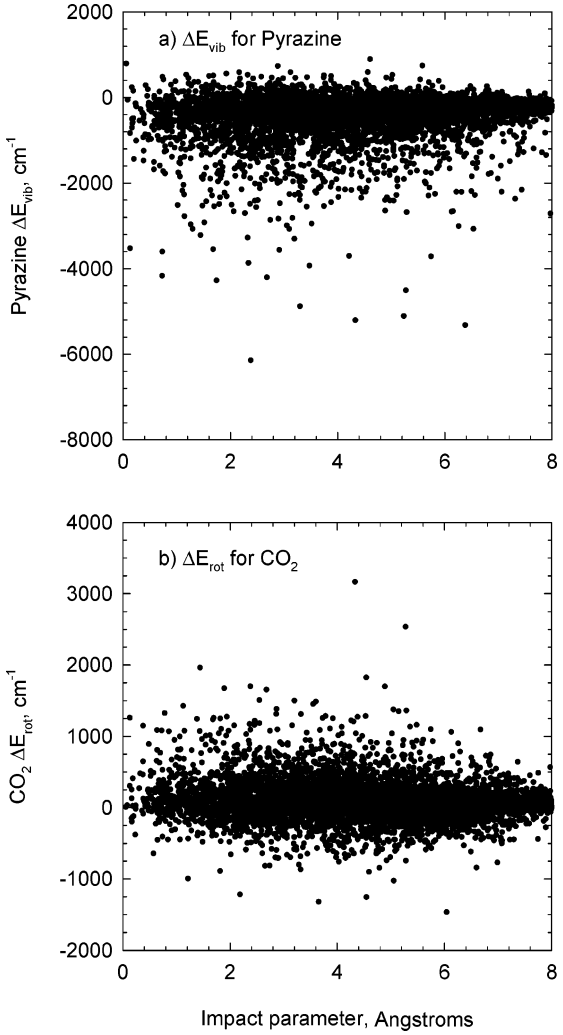

Figure 1. (a) Changes of vibrational energy in the pyrazine donor as a function of impact parameter. (b) Changes of rotational energy in a CO_2 bath as a function of impact parameter. Each point represents one trajectory.

of the relative translational energy with the final CO_2 rotational state. In Figure 4, the data from Figure 3 have been binned by the rotational energy of the scattered CO_2 molecules in increments of 35 cm^{-1} for the trajectories with low rotational energy and 200 cm^{-1} for those with high rotational energy. The two highest rotational energies in Figure 4 correspond approximately to CO_2 rotational levels with $J \sim 50$ and $J \sim 70$. The filled circles in Figure 4 correspond to the average relative translational energy for each rotational increment and demonstrate that on average CO_2 molecules with higher rotational energy are accompanied by larger relative translational energies. The data are fitted by an exponential function, included as a solid line in Figure 4 to guide the eye. It can be seen that as the final CO_2 rotational energy increases, the relative translational energy tends to increase. This finding is in excellent qualitative agreement with the experimental results from our lab[14,16] for pyrazine with E_{vib} = 37 900 cm^{-1} and from Flynn's lab[8] for pyrazine with E_{vib} = 41 000 cm^{-1}. It is interesting to note that translational energies from the calculations are significantly smaller than those measured in the laboratory. For example, our experiments find that scattered CO_2 molecules in the J = 70 state have an average relative translational energy of 2085 cm^{-1} following collisions with hot pyrazine (E_{vib} = 37 900 cm^{-1}), while the trajectory calculations yield a value of E_{rel} = 790 cm^{-1} for CO_2 with a rotational energy corresponding to J

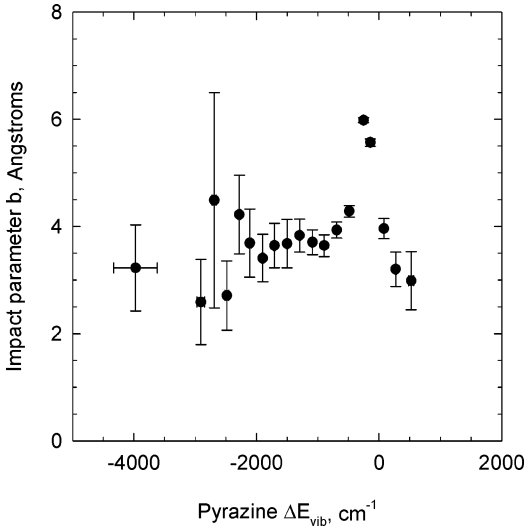

Figure 2. Plot of the impact parameter as a function of the vibrational energy loss in hot pyrazine. Each point represents the average impact parameter for all of the trajectories that fall within a bin of pyrazine vibrational energy loss. The bin size is 200 cm^{-1} for data with low vibrational energy loss, and the last data point corresponds to supercollisions with $|\Delta E_{vib}| > 3000$ cm^{-1}. The error bars represent a 95% confidence level.

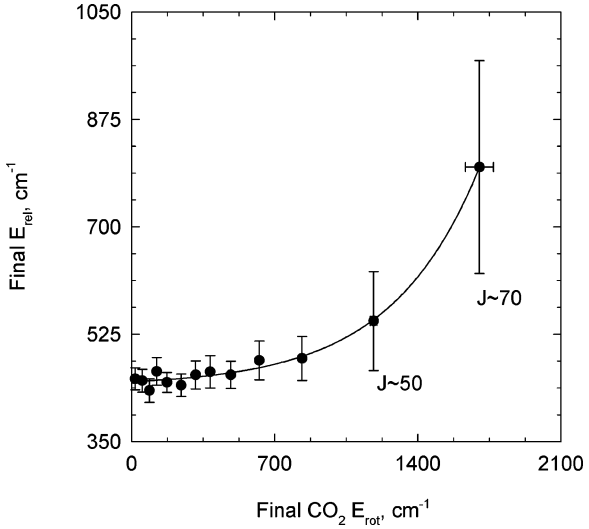

Figure 4. Plot of final relative translational energy vs final CO_2 rotational energy for the randomized microcanonical preparation. Each point represents the average final relative translational energy for all of the trajectories that fall within a bin of CO_2 rotational energy. The energy bin size is 35 cm^{-1} for the trajectories with low rotational energy and 200 cm^{-1} for those with high rotational energy. The error bars represent a 95% confidence level.

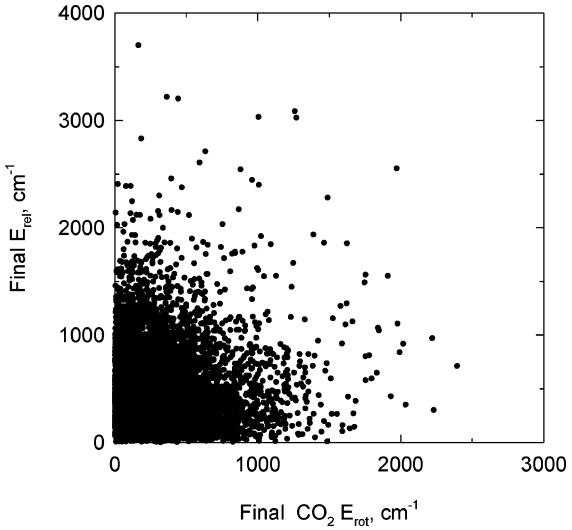

Figure 3. Scatter plot showing the correlation of the final relative translational energy and final CO_2 rotational energy. About 10 000 trajectories are shown in this plot.

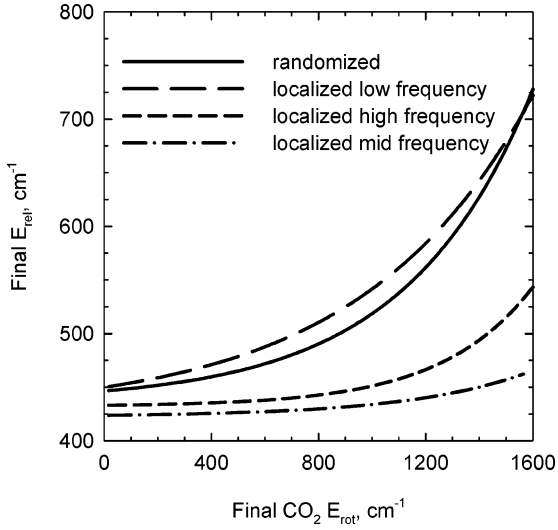

Figure 5. Comparison of randomized vs localized vibration in the hot pyrazine molecule. The results of exponential fitting to the raw data are plotted. The randomized microcanonical and the low-frequency localized trajectories show nearly the same result, while the mid- and high-frequency trajectories show much lower translational energies.

$\sim$ 70. This discrepancy may result from inadequate sampling of the large ΔE collisions or from the harmonic description of pyrazine vibration. In pyrazine molecules with vibrational energy of 37 900 cm^{-1}, the anharmonicity could play an important role in the energy transfer. Future studies will address this issue.

2. Pyrazine (E_{vib}) Vibrational Mode Effects. We now consider how the initial preparation of vibrational energy in pyrazine molecules influences the supercollision excitation of CO_2. We performed a series of calculations on the quenching collisions of hot pyrazine molecules that were prepared with the four different initial vibrational configurations described in section II. The results of 8000−10000 trajectory calculations for each initial preparation of pyrazine vibrational energy are presented in Figure 5. Results for "randomized" pyrazine relaxation are the same as those shown in Figure 4. The "localized low-frequency" preparation gives results that are similar to the randomized preparation and provides the best qualitative agreement with experimental results, particularly for the correlated large rotation/translation energy transfer events. Excitation only in the mid- and high-frequency pyrazine modes leads to substantially smaller amounts of relative translational energy in the scattered molecules. This finding highlights the importance of the low-frequency modes in contributing to supercollision relaxation.

Low-frequency modes are expected to contribute for a number of reasons. The relatively large amplitude motion of the low-frequency modes makes them more likely to encounter the bath molecule than the small amplitude, high-frequency modes. In any statistical distribution, the state density of the low-frequency modes dominates the total state density of the molecule, so using an initial condition which preferentially excites the dominant modes should provide the best description. It is also useful to consider the relative time scales of the two modes involved in the energy transfer for determining the likelihood of the transfer event. If the relative velocity of the approaching molecules is

slow compared to the vibration of a bond, then over the course of the encounter, the relatively high-frequency vibration is averaged out and the impulsive nature of the collision is diminished. In the other extreme, if the relative velocity of the approaching molecules is on a similar time scale as the vibration, then they are more likely to interact impulsively. A typical collisional encounter between pyrazine and CO_2 at 300 K has a duration of ~1 ps. This is the time for the colliding pair to travel ~5 Å relative to the center of mass, which is comparable to the Lennard-Jones diameter for pyrazine and CO_2. A 300 cm^{-1} vibrational mode has a period of about 0.1 ps, while that for a 3000 cm^{-1} mode is 0.01 ps. Under these conditions, the low-frequency modes are expected to contribute more to impulsive collisions leading to effective energy transfer than do the high-frequency modes. This result is in agreement with previous studies using atomic collision partners.[23,24]

3. Anatomy of Strong Collisions with CO_2. Previously Gilbert, Oref, and co-workers[22] simulated the collisional energy transfer from hot azulene to xenon bath molecules and observed large ΔE collisions that involved the xenon interacting in a chattering collision with the hot azulene. They suggested that the energy transfer occurs through multiple interactions between xenon and hot azulene. The "kick" given by the force at the turning point of each encounter governs the amount of energy transferred.

It is informative to look at individual trajectories in order to gain insight into the microscopic dynamics that lead to CO_2 supercollision energy transfer. By looking at simulation movies for those trajectories with large, final CO_2 rotational energy (E_{rot} ~ 1700−2400 cm^{-1}) and/or large, relative translational energy (E_{rel} ~ 2100−3500 cm^{-1}), we see both direct single encounters and multiple encounters (also known as "chattering" collisions). Trajectory movies were analyzed for 24 trajectories with large E_{rel} values, 10 trajectories with large E_{rot} values, 6 trajectories with both large E_{rel} and E_{rot} values, 15 trajectories with $|\Delta E_{vib}| < 600$ cm^{-1}, and 24 trajectories with $|\Delta E_{vib}| > 3000$ cm^{-1}. About 40% of the trajectories with large E_{rot} values in the scattered CO_2 molecules are chattering collisions. About one-third of trajectories with large, final E_{rel} values involve chattering collisions. In our calculations, chattering collisions account for ~50% of trajectories that resulted in both large, final E_{rot} and E_{rel} values. In contrast, for trajectories with both small E_{rot} and E_{trans} values, chattering collisions happen rarely, with only 1 in 15 such trajectories being a chattering collision. This demonstrates that when chattering collisions take place, collisional energy transfer efficiency increases but not all supercollisions are the result of chattering collisions. Linhananta and Lim found similar results for highly vibrationally excited propane and rare gas collisions.[36] Our results illustrate that the number of atom−atom encounters does not necessarily determine the partitioning of energy transferred to bath molecules.

There are many different possible outcomes of collisional energy transfer between polyatomic molecules when one introduces relative orientation. Many of the pyrazine/CO_2 trajectories occur with multiple encounters between pyrazine and CO_2 during a single collision. Here we explore some aspects of such encounters by looking at two representative trajectories, one that is classified as a gentle collision with low $|\Delta E_{vib}|$ and one that is a supercollision with large $|\Delta E_{vib}|$. In Figure 6, we compare the time dependence of the intermolecular potential energy for the two trajectories. The thick line illustrates a gentle collision with $b = 5.9$ Å that results in $\Delta E_{vib} = -475$ cm^{-1}. The thin line corresponds to a supercollision with $b = 2.4$ Å and $\Delta E_{vib} = -4190$ cm^{-1}. The gentle collision results in minor

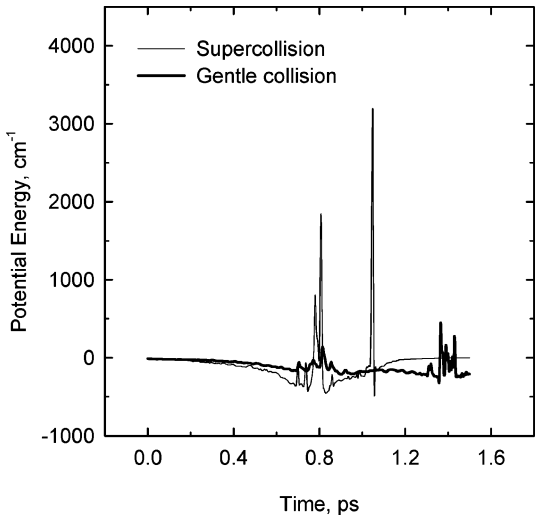

Figure 6. Intermolecular potential energy changes as a function of time for a supercollision with $\Delta E_{vib} = -4190$ cm^{-1} (shown as thin solid line) and a glancing collision with $\Delta E_{vib} = -475$ cm^{-1} (shown as thick solid line). Impact parameter values are $b = 2.37$ Å for the supercollision trajectory and $b = 5.91$ Å for the gentle collision.

increases in translational and rotational energy of the scattered molecules with relatively small changes in the intermolecular potential of ΔE_{pot} ~ 200−500 cm^{-1}. The supercollision trajectory involves much larger changes in potential energy with ΔE_{pot} ~ 2000−3000 cm^{-1}. In both trajectories, there is evidence that attractive forces accelerate the collision partners toward one another and then a series of short-lived repulsive interactions lead to vibrational energy loss from hot pyrazine. The supercollision is complete by 1.5 ps, and the potential energy has approached zero at this time. In contrast, the gentle collision is still involved in an attractive encounter between pyrazine and CO_2 at 1.5 ps. The potential energy spikes that are separated by $t < 100$ fs result from high-frequency vibrational modes (>1000 cm^{-1}) in the hot pyrazine and relative translation of the pyrazine and CO_2. The clumps of potential energy spikes that are spaced by 300−700 fs correspond to relative rotational motion between pyrazine and CO_2 and to low-frequency vibrations in pyrazine.

The role of internal rotation during a representative multiple-encounter supercollision event is illustrated in Figure 7, which shows the relative translational energy between pyrazine and CO_2 as a function of time. A movie of this trajectory along with the data in Figure 7 shows that the first impulsive encounter transfers ~600 cm^{-1} of relative translational energy into rotational energy of the pyrazine, and the CO_2 is left nearly motionless. As the pyrazine molecule rotates and hits the CO_2 again, it transfers nearly 2100 cm^{-1} into translational energy. In this way, the first impulsive encounters serve to reduce the pyrazine/CO_2 relative velocity, and during the second group of impulsive interactions, vibrational energy is funneled out of pyrazine into the recoiling and rotating molecules. It is noteworthy that even though a quasi-complex is formed during the first encounter, internal rotation causes the second encounter to be impulsive with a large change in potential energy, similar to that shown in Figure 6. The trajectory described here represents just one particular sampling of many possible relaxation collisions, but it highlights the importance of intermediate rotational energy transfer. Similar collision-induced internal-rotational energy transfer has been reported by Gilbert and co-workers[22] and by Luther and co-workers.[40]

4. Bath Effects: Mass and Moment of Inertia. Previous state-resolved studies from our labs on collisions of hot pyrazine

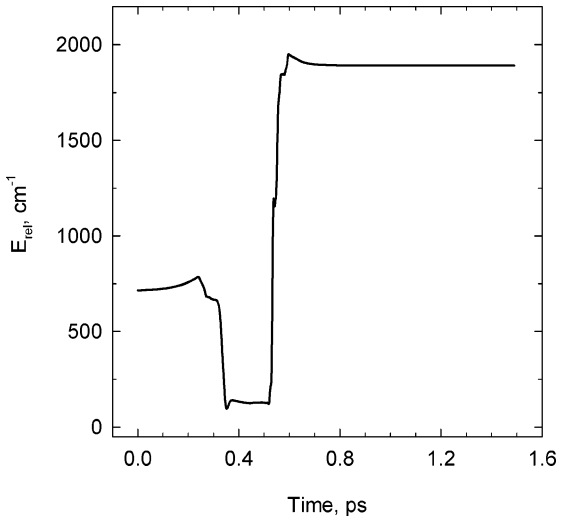

Figure 7. Plot of the relative translational energy vs time for one supercollision trajectory between vibrationally hot pyrazine and CO_2. Initial contact between pyrazine and CO_2 reduces relative velocity to near zero and induces internal rotation in the collision complex. Subsequent impulsive interactions send the pyrazine and CO_2 recoiling and tumbling apart.

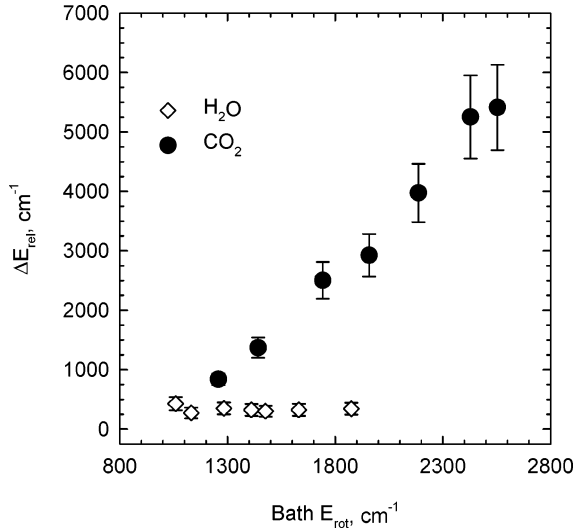

Figure 8. Changes of relative translational energy gain in bath molecules as a function of final rotational energy in bath molecules from diode probing experiments on pyrazine relaxation (refs 14, 15, and 16). Bath molecules are CO_2 and H_2O.

(E_{vib} = 37 900 cm^{-1}) with various small bath molecules have revealed that the mass and/or moments of inertia of the bath molecule influence the partitioning of rotational and translational energy gain in bath molecules.[15,20] This observation is illustrated by the experimental results shown in Figure 8. For CO_2 and H_2O, there is a significant difference in the amount of translational energy released as a result of collisions with hot pyrazine. We find that the translational energy component of the released energy correlates with the change in angular momentum for the bath molecule, which increases with the increasing moment of inertia of the bath.[20] There is also a mass difference between CO_2 and H_2O which would influence the relaxation behavior via an orbital angular momentum effect. However, recent experiments using DCl as a quencher reveal that the energy partitioning in scattered DCl molecules is much closer to those for H_2O than that for CO_2, even though the masses of DCl and CO_2 are similar. This suggests that moment of inertia may have a larger effect on energy partitioning than that of mass alone.

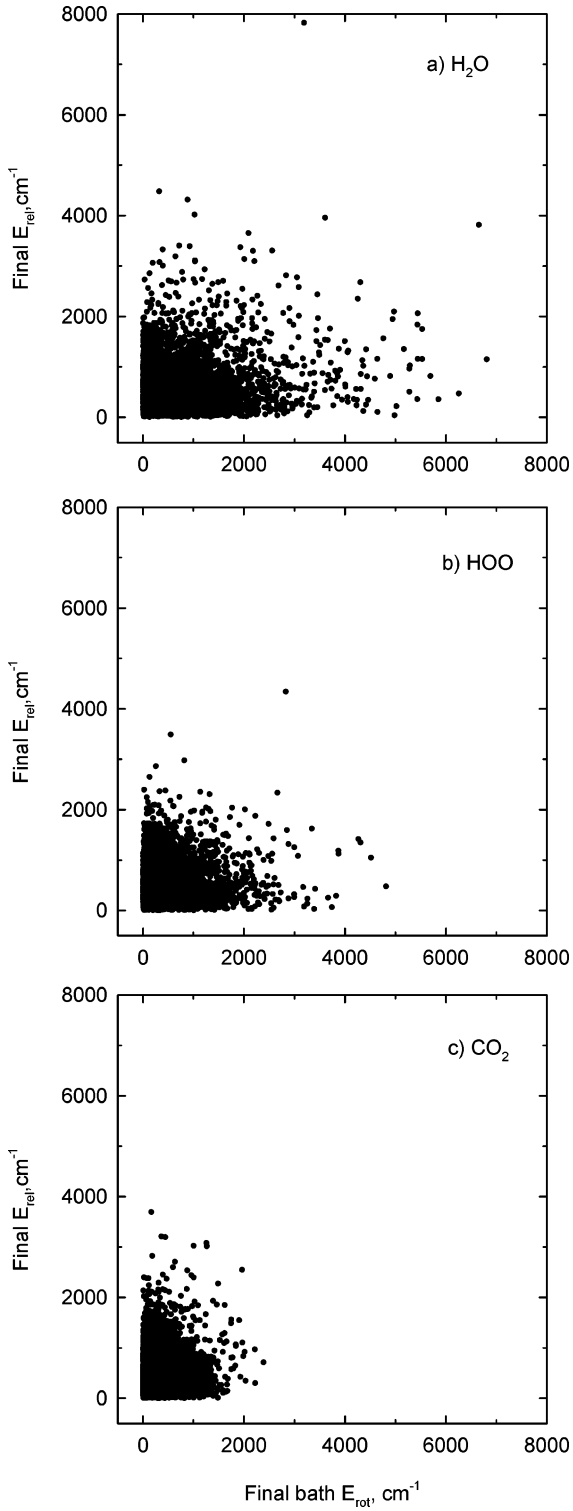

Figure 9. Scatter plots showing the correlation of final relative translational energy and final bath rotational energy for (a) H_2O, (b) HOO, and (c) CO_2. There are about 10 000 trajectories in each plot.

To test bath effects through simulations, we formed pseudo-H_2O and pseudo-HOO using the potentials, configurations, and size of CO_2 and replacing the atomic masses of CO_2 with those for H_2O and HOO. We studied the collisional relaxation of hot pyrazine (E_{vib} = 37 900 cm^{-1}) by "linear H_2O" and "linear HOO". We performed ~10 000 trajectory calculations for each bath molecule, and the results are shown in Figure 9. The results show that all three bath molecules gain both rotational and translational energy during collisions with vibrationally hot

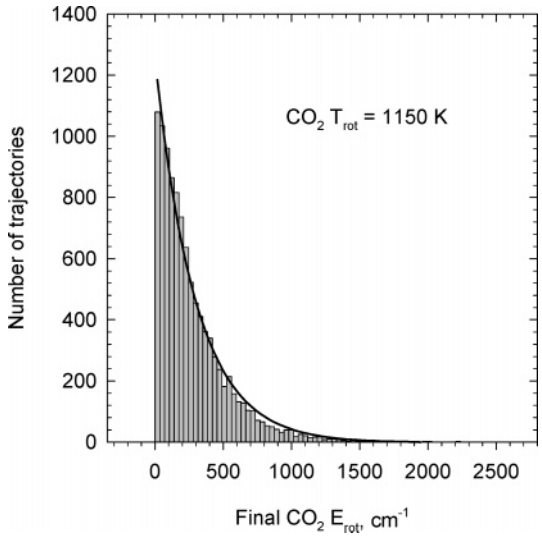

Figure 10. Histogram of CO_2 rotational energy showing the number of trajectories as a function of CO_2 final rotational energy.

pyrazine, but the energy gain partitioning is dependent upon the bath identity. Figure 9 shows that the fraction of energy that goes into translation of the scattered molecules increases in the order of "linear H_2O" < "linear HOO" < CO_2. This ordering is consistent with recent experimental data from our labs in which the energy partitioning between rotation and translation has been explained in terms of angular momentum constraints.[20] Through conservation of rotational and orbital angular momentum in collisions, the extent of recoil velocity imparted to the departing molecules is proportional to rotational angular momentum changes that occur during the collision. For similar ΔE_{rot} values, bath molecules with smaller moments of inertia have larger energy gaps between rotational states, exhibit smaller ΔJ values in collisions, and have smaller recoil velocities than bath species with larger moments of inertia. The three bath molecules considered here have essentially the same properties except for their moments of inertia which increase as $I_{\text{linear } H_2O} < I_{\text{linear HOO}} < I_{CO_2}$. Our simulations show that H_2O molecules, which have the smallest moment of inertia, preferentially gain energy into rotation relative to translation, while CO_2 molecules with the largest moment of inertia gain a relatively larger proportion in translational energy. The partitioning for HOO lies between that for H_2O and CO_2. This behavior is in excellent qualitative agreement with our experimental trends. Future simulations will address the comparative roles that mass and moment of inertia play by using bath molecules with the same total mass but different moments of inertia.

5. Rotational and Translational Temperature of Scattered CO_2. We now consider the CO_2 rotational and translational energy gain in more detail. The histogram of rotational energy gain in CO_2 is displayed in Figure 10 and shows the number of trajectories as a function of the rotational energy of the scattered CO_2 molecules. We fit the simulated rotational population data using a Boltzmann distribution

$$\frac{\text{Population}}{g} = \exp\left(\frac{-E_{rot}}{k_B T_{tot}}\right) \tag{6}$$

where k_B is Boltzmann's constant and g is the rotational degeneracy. The rotational degeneracy ($g = 2J + 1$) was determined by equating the CO_2 rotational energy to $E_{rot} = BJ(J + 1)$ and solving for the nearest J value. The data in Figure 10 were fitted to eq 6 and yielded a rotational temperature of T_{rot} = 1150 K for pyrazine/CO_2 with $J = 54-74$. This result is very close to our experimental result of $T_{rot} = 1200$ K.[16]

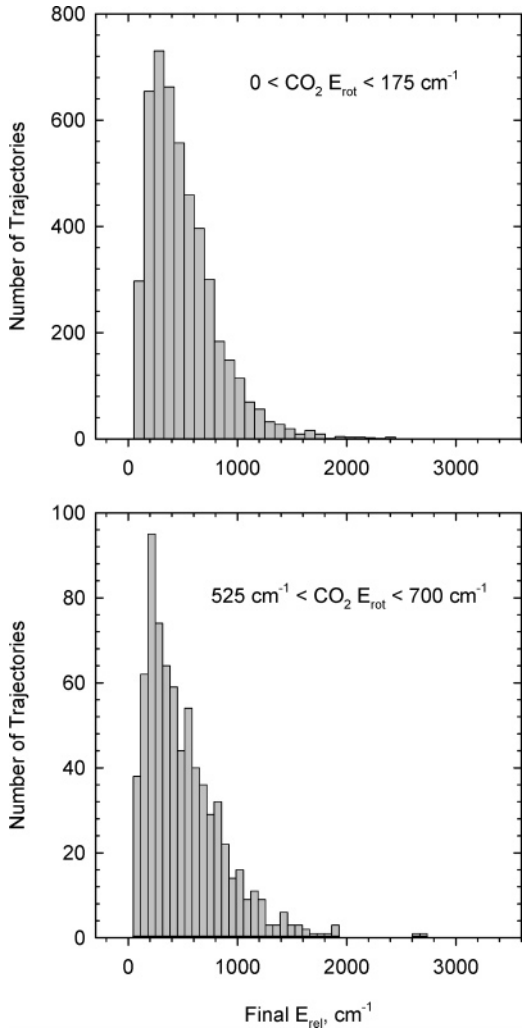

Figure 11. Distributions of final translational energy for different ranges of final CO_2 rotational energy. The upper panel is for $E_{rot} = 0-175$ cm^{-1}, and the lower panel is for $E_{rot} = 525-700$ cm^{-1}.

Figure 11 shows the distribution of final relative translational energy for two different ranges of rotational energy in CO_2. One sees that for low and high rotational energies, CO_2 gains both translational energy and rotational energy. A comparison of the number of trajectories for the two plots demonstrates that supercollision energy transfer with large E_{rot} values is a relatively low probability event. The final relative translational energy distribution for pyrazine/CO_2 collisions, averaged over all rotational energies, is shown in Figure 12 where the logarithm of the number of trajectories per bin divided by its mean translational energy is shown as a function of E_{rel}. Two distinct distributions are seen in Figure 12, both of which are fit using a Boltzmann distribution[47] at temperature T_{rel} In eq 7, $P(E_{rel})$ is

$$P(E_{rel}) = \frac{E_{rel}}{(k_B T_{rel})^2} \exp\left(\frac{-E_{rel}}{k_B T_{rel}}\right) \tag{7}$$

the probability per cm^{-1} that collisions result in E_{rel} of the scattered molecules. The lower energy portion is well described by a translational temperature of $T_{rel} = 340$ K. The higher energy tail has a translational temperature of $T_{rel} = 900$ K, which qualitatively agrees with our experimental results. The magnitude of translational energy gain, ΔE_{rel}, in the simulations is

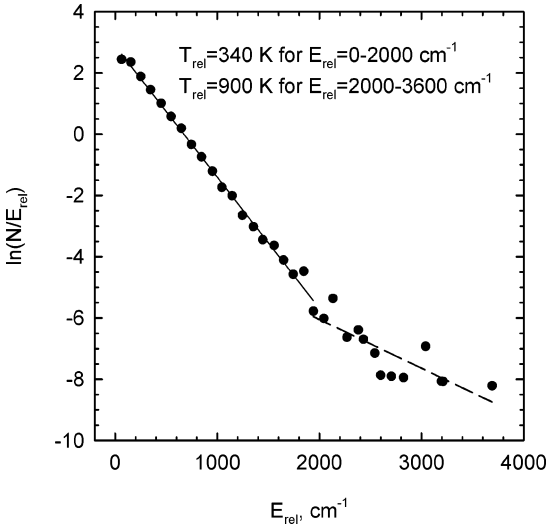

Figure 12. Final translational energy distribution averaged over all J states. The lower energy portion with $E_{rel} = 0-2000$ cm^{-1} is fit to thermal distribution with $T_{rel} = 340$ K. The higher energy tail yields $T_{rel} = 900$ K for $E_{rel} = 2000-3600$ cm^{-1}.

substantially smaller than that in our experiments. Since supercollision relaxation is relatively rare, this discrepancy could be due to insufficient sampling rates in the simulations. It may also be that more accurate descriptions of the potential energy and the coupling between modes in pyrazine would improve the agreement between experiment and theory.

IV. Conclusions

Classical trajectory calculations on the supercollision relaxation of highly vibrationally excited pyrazine ($E_{vib} = 37\,900$ cm^{-1}) with CO_2 qualitatively reproduce experimental results from state-resolved studies. The simulation results are in excellent agreement with the experimentally observed distribution of rotational energy gain for CO_2. They also successfully reproduce the experimentally observed correlation of rotational and translational energy in scattered CO_2 molecules. The extent of translational energy in the scattered molecules determined in the simulations is less than that observed in the lab, which may result from insufficient sampling of the rare supercollision events or from an incomplete description of the potential energy. This illustrates one of the challenges in simulating physical processes that occur with low probability.

The simulations reported here also provide insight into the nature of highly excited molecules. We have found that strong collisions are more likely when low-frequency, large-amplitude motions are populated in the excited donor molecules. The simulations show that chattering collisions involving multiple impulsive encounters for a donor and acceptor pair contribute to supercollision relaxation. The simulations exploring effects of mass and moment of inertia in the energy accepting bath molecule qualitatively reproduce experimental results showing that energy gain partitioning is influenced by the moment of inertia in the bath molecule. This result provides additional data indicating that angular momentum is important in determining the partitioning of energy gain in bath molecules in supercollision relaxation. The studies reported here demonstrate that classical trajectories are a useful means of understanding supercollision relaxation by complementing state-resolved transient IR energy transfer studies. This integrated approach leads to a better understanding of the interactions and molecular properties that control the relaxation of high-energy molecules.

Acknowledgment. This work is dedicated to Prof. George W. Flynn in honor of his 65th birthday. The authors thank Profs. K. Luther and K. Lim and Drs. T. Lenzer and U. Grigoleit for providing potentials and helpful computer code. A.S.M. received support as a Camille Dreyfus Teacher Scholar. R.L.S. received support from the Boston University Undergraduate Research Opportunities Program. This work was performed at Boston University. The technical development used in the simulations was supported by the National Science Foundation (CHE-0079146 and CHE-0316836) and the American Chemical Society (ACSPRF 39180-AC6), and the simulations were supported by the Department of Energy (DE-FG-03ER15429).

Supporting Information Available: Appendix A gives the diagonal parameters for pyrazine intramolecular potential, appendix B gives the parameters for CO_2 intramolecular potential, and appendix C gives Lennard-Jones potential parameters. This material is available free of charge via the Internet at http://pubs.acs.org.

References and Notes

(1) Oref, I.; Tardy, D. C. *Chem. Rev.* **1990**, *90*, 1407.
(2) Flynn, G. W.; Parmenter, C. S.; Wodtke, A. M. *J. Phys. Chem.* **1996**, *100*, 12817.
(3) Mullin, A. S.; Schatz, G. C.; Eds. *Highly Excited Molecules: Relaxation, Reaction, and Structure*; ACS Symposium Series 678; Americal Chemical Society: Washington DC, 1996.
(4) Miller, L. A.; Barker, J. R. *J. Chem. Phys.* **1996**, *105*, 1383.
(5) Yerram, M. L.; Brenner, J. D.; King, K. D.; Barker, J. R. *J. Phys. Chem.* **1990**, *94*, 6341.
(6) Hippler, H.; Lindemann, L.; Troe, J. *J. Chem. Phys.* **1985**, *83*, 3906.
(7) Lenzer, T.; Luther, K.; Reihs, K.; Symonds, A. C. *J. Chem. Phys.* **2000**, *112*, 4090.
(8) Mullin, A. S.; Park, J.; Chou, J. Z.; Flynn, G. W.; Weston, R. E., Jr. *Chem. Phys.* **1993**, *175*, 53.
(9) Mullin, A. S.; Michaels, C. A.; Flynn, G. W. *J. Chem. Phys.* **1995**, *102*, 6032.
(10) Michaels, C. A.; Mullin, A. S.; Flynn, G. W. *J. Chem. Phys.* **1995**, *102*, 6682.
(11) Michaels, C. A.; Lin, Z.; Mullin, A. S.; Tapalian, H. C.; Flynn, G. W. *J. Chem. Phys.* **1997**, *106*, 7055.
(12) Michaels, C. A.; Mullin, A. S.; Park, J.; Chou, J. Z.; Flynn, G. W. *J. Chem. Phys.* **1998**, *108*, 2744.
(13) Sevy, E. T.; Rubin, S. M.; Lin, Z.; Flynn, G. W. *J. Chem. Phys.* **2000**, *113*, 4912.
(14) Wall, M. C.; Mullin, A. S. *J. Chem. Phys.* **1998**, *108*, 9658.
(15) Fraelich, M.; Elioff, M. S.; Mullin, A. S. *J. Phys. Chem. A* **1998**, *102*, 9761.
(16) Wall, M. C.; Lemoff, A. E.; Mullin, A. S. *J. Chem. Phys.* **1999**, *111*, 7373.
(17) Elioff, M. S.; Fang, M.; Mullin, A. S. *J. Chem. Phys.* **2001**, *115*, 6990.
(18) Park, J.; Shum, L.; Lemoff, A. S.; Werner, K.; Mullin, A. S. *J. Chem. Phys.* **2002**, *117*, 5221.
(19) Park, J.; Li, Z.; Lemoff, A. S.; Rossi, C.; Elioff, M. S.; Mullin, A. S. *J. Phys. Chem. A* **2002**, *106*, 3642.
(20) Li, Z.; Korobkova, E.; Werner, K.; Shum, L.; Mullin, A. S. *J. Chem. Phys.*, submitted for publication.
(21) Clarke, D. L.; Thompson, K. C.; Gilbert, R. G. *Chem. Phys. Lett.* **1991**, *182*, 357.
(22) Clarke, D. L.; Oref, I.; Gilbert, R. G.; Lim, K. F. *J. Chem. Phys.* **1992**, *96*, 5983.
(23) Clary, D. C.; Gilbert, R. G.; Bernshtein, V.; Oref, I. *Faraday Discuss.* **1995**, 423.
(24) Lenzer, T.; Luther, K.; Troe, J.; Gilbert, R. G.; Lim, K. F. *J. Chem. Phys.* **1995**, *103*, 626.
(25) Koifman, I.; Dashevskaya, E. I.; Nikitin, E. E.; Troe, J. *J. Phys. Chem.* **1995**, *99*, 15348.
(26) Lenzer, T.; Luther, K. *J. Chem. Phys.* **1996**, *105*, 10944.
(27) Bruehl, M.; Schatz, G. C. *J. Phys. Chem.* **1988**, *92*, 7223.
(28) Schatz, G. C.; Lendvay, G. *J. Chem. Phys.* **1997**, *106*, 3548.
(29) Lendvay, G.; Schatz, G. C. *J. Phys. Chem.* **1991**, *95*, 8748.
(30) Brunsvold, A. L.; Garton, D. J.; Minton, T. K.; Troya, D.; Schatz, G. C. *J. Chem. Phys.* **2004**, *121*, 11702.
(31) Bernshtein, V.; Oref, I. *J. Chem. Phys.* **2003**, *118*, 10611.
(32) Bernshtein, V.; Oref, I. *J. Phys. Chem. A* **2001**, *105*, 10646.
(33) Bernshtein, V.; Oref, I. *Chem. Phys. Lett.* **1999**, *300*, 104.
(34) Lim, K. F. *J. Chem. Phys.* **1994**, *100*, 7385.

(35) Lim, K. F. *J. Chem. Phys.* **1994**, *101*, 8756.
(36) Linhananta, A.; Lim, K. F. *Phys. Chem. Chem. Phys.* **2002**, *4*, 577.
(37) Bernshtein, V.; Oref, I. *J. Phys. Chem. B* **2005**, *109*, 8310.
(38) Grigoleit, U.; Lenzer, T.; Luther, K. *Z. Phys. Chem. (Muenchen)* **2000**, *214*, 1065.
(39) Grigoleit, U.; Lenzer, T.; Luther, K.; Mutzel, M.; Takahara, A. *Phys. Chem. Chem. Phys.* **2001**, *3*, 2191.
(40) Lenzer, T.; Luther, K. *J. Chem. Phys.* **1996**, *104*, 3391.
(41) Higgins, C.; Ju, Q.; Seiser, N.; Flynn, a. G. W.; Chapman, S. *J. Phys. Chem. A* **2001**, *105*, 2858.
(42) Higgins, C. J.; Chapman, S. *J. Phys. Chem. A* **2004**, *108*, 8009.
(43) Yoder, L. M.; Barker, J. R. *J. Phys. Chem. A* **2000**, *104*, 10184.
(44) Seiser, N.; Kavita, K.; Flynn, G. W. *J. Phys. Chem. A* **2003**, *107*, 8191.
(45) Yoder, L. M.; Barker, J. R. *Phys. Chem. Chem. Phys.* **2000**, *2*, 813.
(46) Zalesskaya, G. A.; Yakovlev, D. L.; Sambor, E. G.; Prikhodchenko, D. V. *Opt. Spectrosc.* **2001**, *90*, 526.
(47) Hase, W. L.; Duchovic, R. J.; Hu, X.; Komornicki, A.; Lim, K. F.; Lu, D.-H.; Peslherbe, G. H.; Swamy, K. N.; Linde, S. R. V. d.; Varandas, A.; Wang, H.; Wolf, R. J. *VENUS96, a General Chemical Dynamics Computer Program*; 1996.
(48) Grigoleit, U. Chapter 8 and Appendix. Ph.D. Thesis, 1998.
(49) Zarembowitch, J.; Bokobza-Sebagh, L. *Spectrochim. Acta, Part A* **1976**, *32A*, 605.
(50) Herzberg, G. *Infrared and Raman Spectra of Polyatomic Molecules*; D. Van Nostrand: New York, 1945.
(51) Beyer, T.; Swinehart, D. F. *Comm. Assoc. Comput. Machines* **1973**, *16*, 379.
(52) Stein, S. E.; Rabinovitch, B. S. *J. Chem. Phys.* **1973**, *58*, 2438.